Rare Metal Materials and Engineering
Volume 48, Issue 6, June 2019
Available online at www.rmme.ac.cn

Science Press

Cite this article as: Rare Metal Materials and Engineering, 2019, 48(6): 1725-1733.

ARTICLE

Corrosion Behavior and Mechanical Properties of FHAP/MAO Composite Coating on Pure Titanium Substrate Prepared by Micro-arc Oxidation and Electrochemical Deposition

Jin Jie, Zhou Shuwei, Zheng Dacai

Zhejiang University of Technology, Hangzhou 310014, China

Abstract: A fluorine-doped hydroxyapatite (FHAP)/micro-arc oxidation (MAO) composite coating was deposited on commercially pure titanium (CPTi) surface through micro-arc oxidation and electrochemical deposition (ED) technique. Simulative Hank's solution was used to test the electrochemical corrosion resistance of uncoated CPTi substrate and coated samples. The effect of MAO interface layer on the micro-structure, mechanical property, and electrochemical property of the coating was studied. Results show that the deposited HAP/Ti, FHAP/Ti and FHAP/MAO/Ti coating samples dramatically improve the anticorrosion of the CPTi substrate in the simulative Hank's solution. However, the mechanical properties testing shows that FHAP/Ti coating has a poor bonding strength of 10.7 MPa compared to FHAP/Ti coating with a MAO interface layer (18.1 MPa). Furthermore, the contact angle of the FHAP/MAO/Ti coating with deionized water is approximately 35.8°, which is more beneficial to promoting cell attachment and proliferation.

Key words: hydroxyapatite; micro-arc oxidation; corrosion resistance; electrochemical test; contact angle

Commercially pure titanium (CPTi) and titanium alloys are the most generally used metal material for medical implants in the field of orthopedic and dental applications because of their good biocompatibility, acceptable mechanical properties, and high resistance to corrosion [1]. However, it has been reported that these implants cause an avascular fibrous tissue inflammatory response that encapsulates the implants[2]. Therefore, various bioactive coatings have been proposed to improve the osseointegration and stability of CPTi or titanium alloys. Hydroxyapatite ($Ca_5(PO_4)_3OH$, HAP) is the preferred coating to assist the osseointegration of these implants with surrounding tissues and it can prevent inflammation by improving the chemical bonding between HAP film and regenerated bone[3,4]. However, the dissolution rate of pure HAP coating is high in a biological environment, which has a strong negative effect on the stability of the implants and makes HAP films gradually fail and flake off[5,6]. Therefore, fluorine-doped hydroxyapatite ($Ca_{10}(PO4)_6(OH)_{2-x}F_x$ ($0<x<2$), FHAP) has been widely researched as a promising candidate for replacing HAP coatings due to its significant dissolution-resistant property and good alkaline phosphatase activity in cell culture[7,8].

Various techniques and methods of depositing HAP or FHAP on the surface of CPTi and its alloys have been studied, including plasma-spraying[9], collosol-gelling method[10], electrophoretic deposition[11], and electrochemical methods[12]. Plasma-spraying is a commonly used technique. However, the high working temperature can lead to decomposition and phase transformation of HAP[13], and this method also has some underlying problems, including the presence of residual stress in HAP coatings, exposure of substrates to high temperature, and the inability to coat the parts with complicated cavities[14]. Electrochemical deposition (ED) is regarded as one of the effective methods for the surface

Received date: June 10, 2018
Corresponding author: Jin Jie, Ph. D., Professor, College of Materials Science and Engineering, Zhejiang University of Technology, Hangzhou 310014, P. R. China, E-mail: jiejinzjut@sina.com

modification because of low processing temperature, porous or complex shapes of substrate and low-cost equipment[15]. Nevertheless, HAP coating prepared by ED has a relatively high dissolution rate and a poor interface bonding strength between HAP and Ti, which restricts the further application of ED. In particular, the composite coating of HAP/MAO is often proposed as an effective way for improving corrosion performance and cellular integration in biological environment[16,17]. Micro-arc oxidation (MAO) can effectively improve the corrosion resistance by forming a ceramic coating on metals. Previous studies have suggested that MAO can allow the incorporation of Ca and P into the surface oxide when suitable electrolytes are used[18,19]. Therefore, porous MAO film provides adequate support for the adhesion of HAP particles to improve their mechanics performance for biomedical applications in the structure of HAP/MAO.

CPTi was used as the substrate material for supporting the HAP/Ti, FHAP/Ti, and FHAP/ MAO/Ti coatings due to its excellent mechanics performance, and the functional FHAP/ MAO composite coatings were fabricated through a combination of MAO and ED technique. The corrosion behavior and mechanical properties of FHAP/MAO composite coating were investigated to improve dissolution-resistant property and to get some basic and essential information for the development of FHAP/MAO bioactive coating as medical implants.

1 Experiment

1.1 Coating preparation

CPTi sheets with a size of 10 mm×10 mm×2 mm were used as the substrate material. The CPTi discs were polished by different grinding papers (600#, 800#, 1000#, 1200#), and etched in 20% (*v*/*v*) solution of hydrofluoric acid for 30 s. After treatments above, the samples were ultrasonically cleaned in anhydrous ethanol and acetone for 15 min, washed twice with distilled water and finally dried in air. A MAO operating unit (DSM35F) was used to prepare ceramic coating. The MAO film was fabricated in 10 g/L $Na_3PO_4{\cdot}12H_2O$, 10 g/L $Na_2SiO_3{\cdot}9H_2O$, 1.5 g/L CaF_2, and 2 g/L NaOH solution under constant current mode of 20 mA/cm^3 for 20 min at 20~30 °C. After the MAO process, the samples were ultrasonically cleaned in distilled water and dried in air.

FHAP/MAO films were deposited by an electrochemical deposition method. The electrolyte includes 0.042 mol/L $Ca(NO_3)_2$, 0.0008 mol/L NaF and 0.025 mol/L $NH_4H_2PO_4$. The pH value of the electrolyte was adjusted to 4 using dilute nitric acid solution, and the electrodeposition was performed at the temperature of 65 °C and a current density of 0.49 mA/cm^2 for 90 min. Electrochemical deposition was carried out by electrochemical workstation (IVIUMSTAT). The MAO coated samples served as the cathode, a saturated calomel electrode (SCE) served as the reference electrode, and a platinum sheet served as the counter electrode. After electrochemical deposition, the coated samples were rinsed with deionized water and dried at room temperature for 24 h. The coated samples were then annealed at 550 °C for 2 h in the argon atmosphere (heating rate=10 °C/min, argon flow rate= 200 cm^3/min). For comparison, FHAP/Ti and HAP/Ti coated samples were designated as control samples.

1.2 Coating surface analysis

The construction and the relative crystallinity of as-received samples were detected by X-ray diffraction (Panalytical X'pert PRO). The surface morphology and the thickness of coated samples were examined using scanning electron microscopy (TESCAN VEGA3). In addition, the microhardness and elastic modulus of coated samples were determined using a nano-indenter (Nano Indenter G200). The contact angles of coated and uncoated samples with deionized water were measured by Dataphysics OCA30 angle measurement system.

1.3 Electrochemical corrosion measurement

The electrochemical experiments include electrochemical impendence spectroscopy (EIS) and potentiodynamic polarization measurement (PDP). All the tested samples were tested in Hank's solution (8 g/L NaCl, 0.4 g/L KCl, 0.25 g/L $NaH_2PO_4{\cdot}H_2O$, 0.19 g/L $CaCl_2{\cdot}2H_2O$, 0.35 g/L $NaHCO_3$, 0.06 g/L $Na_2HPO_4{\cdot}2H_2O$, 0.06 g/L $MgSO_4{\cdot}7H_2O$ and 1 g/L glucose, pH=7.8) at room temperature. The electrochemical measurements were carried out by electrochemical workstation. A saturated calomel electrode (SCE) was used as the reference electrode, the sample with an exposed surface area of 3.14 cm^2 was used as the working electrode, and a platinum sheet was used as the counter electrode. Before the electrochemical measurements, the samples were immersed into the electrolyte for 30 min at open circuit potential (OCP) in order to maintain electrochemical stabilities. The PDP test was measured at a scanning rate of 1 mV·s^{-1}, and the potential was increased from −2.0 V to 1.0 V (vs. SCE). The EIS measurement was researched in a frequency range of 10^5~10^{-2} Hz with the perturbation amplitude of ±10 mV.

1.4 Adhesion strength testing

The bonding strength of coated samples was measured by ASTMC633[20]. The uncoated surface of the CPTi discs was polished and glued to the stubs and the coated surface of the CPTi discs was glued to metal rod by high performance epoxy resin. The schematic diagram is shown in Fig.1. Two stubs were aligned vertically and the bonding strength of the coated samples was tested by a tensile machine (Instron 8801, American) at a tensile rate of 0.1 mm/min. The critical load *F* was recorded when the coatings were desquamated. The tensile strength (σ_F) can be obtained by Eq. (1):

$$\sigma_F = \frac{F}{S} = \frac{4F}{\pi d^2} \quad (1)$$

where *d* represents the diameter of CPTi disc. In addition, each testing was repeated three times and the data were averaged.

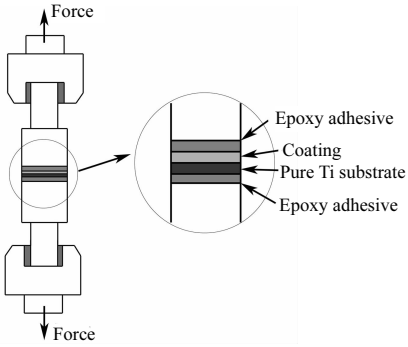

Fig.1 Schematic diagram of the bonding strength test

2 Results and Discussion

2.1 Surface topography analysis

Surface morphologies of MAO/Ti, HAP/Ti, FHAP/Ti, and FHAP/MAO/Ti on CPTi substrates are shown in Fig.2. Fig.2a shows that small porous structures (<10 μm in diameter) form on the surface after MA treatment. The SEM image of HAP/Ti coating shows that the substrates are covered by an HAP film with homogenous and dense structure. In addition, the HAP/Ti coating shows that the microstructure of the HAP layer is a typical needle-like crystal with a growth direction perpendicular to the substrate surface and some cotton-like HAP appears above the needle-like HAP layer (Fig.2b). According to the analysis of He et al[21], the formation of the cotton-like HAP can be attributed to the precipitation of the needle-like HAP crystal during electrochemical deposition process. The density of the needle-like HAP crystal is low and some interspaces are formed in the surface of HAP layer at the beginning of the deposition, which would make electrochemical reactions more likely to take place in these gaps. The pH value near gaps increases as the stronger electrochemical reaction progresses, thus accelerating the increase trend of new nucleation and eventually promoting the development of the cotton-like HAP. The FHAP/Ti consists mainly of nano-hydroxyapatite crystals in needle-like appearance, and the magnified image shows a flower-like structure. FHAP/MAO/Ti coating exhibits similar morphology (inset in Fig.2c and 2d). The needle crystals of HAP are sparse, and the FHAP/Ti and FHAP/MAO/Ti are relatively thin and dense. The flower-like structure of FHAP/Ti is more obvious than that of FHAP/MAP/Ti, and is more numerous. Its number is larger, but its size is smaller. This is because MAO surface is rough, and more flower-like structure can be formed during growing, while they squeeze each other so it is hard to form a flower-like structure.

2.2 Cross-sectional SEM and EDS analyses

The cross-sectional SEM images of the HAP/Ti, FHAP/Ti and FHAP/MAO/Ti are displayed in Fig.3. The thickness range of HAP/Ti, FHAP/Ti and FHAP/MAO/Ti coatings is 8~10 μm. The section morphology of all the samples is similar, needle-like HAP and FHAP crystal are perpendicular to the substrate, and the arrangement of the needle-like crystal is close. The insets in Fig.3a~3c show the EDS spectra of HAP or FHAP layer on CPTi substrate. It clearly shows the percentage of P, Ca, O etc in HAP, FHAP and FHAP/MAO films. The Ca/P atomic ratios of the HAP coated sample is about 1.73, higher than the standard value (1.67), indicating that the HAP/Ti coated sample is P insufficient. With the

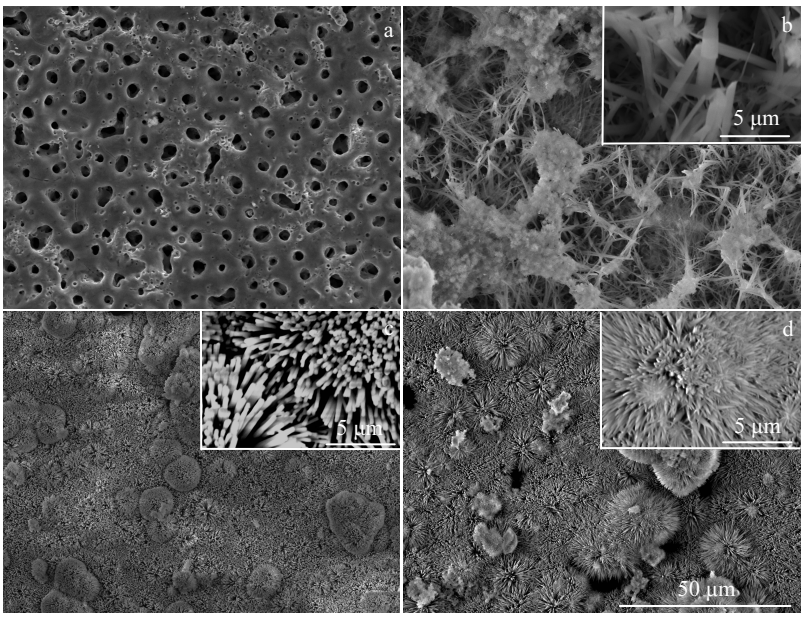

Fig.2 Surface morphologies of MAO/Ti (a), HAP/Ti (b), FHAP/Ti (c), and FHAP/MAO/Ti (d)

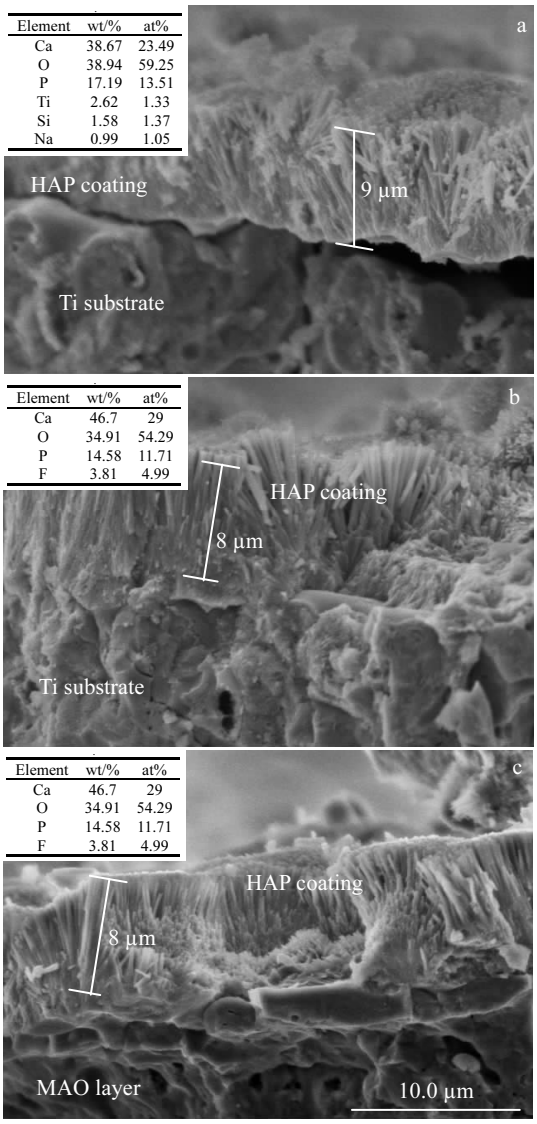

Fig.3 Cross-sectional morphologies and EDS analysis of CPTi (a), FHAP/Ti (b), and FHAP/MAO/Ti (c)

addition of fluorine in the HAP coating, the percentages of Ca increased from 38.67 wt% to 46.7 wt%, and the percentages of P decreased from 17.19 wt% to 14.58 wt% (Fig.3a and 3b). The Ca/P atom ratio increased from 1.73 to 2.47, and the signal increase of 44% in Ca/P atom ratio indicates the surface composition change with the addition of fluorine in the HAP coating. However, the Ca/P atom ratio of FHAP/MAO/Ti composite coating decreased from 2.47 to 1.88 (Fig.3c), which indicates that the intermediate MAO layer results in a significant promotion in the formation of HAP compared to the direct FHAP coating on CPTi without MAO treatment.

2.3 XRD analysis

Fig.4 shows XRD patterns of the HAP/Ti, FHAP/Ti and FHAP/MAO/Ti. It shows that all diffraction peaks can be indexed readily to the standard HAP, FHAP, and Ti patterns.

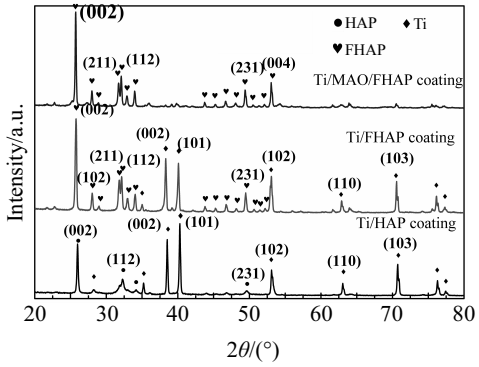

Fig.4 XRD patterns of HAP/Ti, FHAP/Ti and FHAP/MAO/Ti

The Ti (002), Ti (101), and Ti (102) substrate diffraction peaks come from HAP/Ti and FHAP/Ti coatings, and the appearance of Ti in HAP/Ti and FHAP/Ti indicates that X-ray can penetrate through the whole thin coatings deposited on the pure Ti. After MAO layer is coated, Ti diffraction peaks disappear. Similarly, no typical titanium oxide peaks were found in the FHAP/MAO/Ti. The peaks at 25°~37° are the main characteristic peaks of HAP phase. The FHAP/Ti diffraction peaks are composed of the FHAP phase and the hcp-Ti phase, and the appearance of FHAP reflections existing in FHAP/Ti and FHAP/MAO/Ti indicates that F ions are incorporated into the crystal structure of HAP by replacing the H with F, thereby forming FHAP[22]. Fig.4 also shows that fluorine ion doping in a small quantity can effectively improve the crystallinity of hydroxyapatite.

2.4 Potentiodynamic test

Fig.5 shows the polarization curves of uncoated CPTi and modified samples (MAO/Ti, HAP/Ti, FHAP/Ti and FHAP/MAO/Ti) in Hank's solution. The corrosion current density (i_{corr}) and corrosion potential (E_{corr}) of the coated samples can be calculated by the mean of linear polarization, as summarized in Table 1. i_{corr} and E_{corr} values show that the uncoated CPTi and modified CPTi samples have different corrosion rates. The E_{corr} values of the uncoated CPTi and MAO/Ti are −573 mV (vs. SCE) and −467 mV (vs. SCE), respectively. Compared with MAO/Ti, the uncoated CPTi has a more negative E_{corr}. This result is similar to previous research results[23,1]. The MAO coating is composed of thick outer loose layer and thin inner compact layer, and the inner layer can considerably inhibit the corrosion of substrate when samples are immersed in chloride solution[24]. In addition, a significant increase in the E_{corr} from −467 mV (vs. SCE) to −407 mV (vs. SCE) was observed after uniform FHAP coating was formed on MAO film. This indicates that the incorporation of uniform FHAP layer improves the corrosion resistance of the MAO coating. As the dense FHAP layer was formed on MAO coating, more pores were blocked, which can obviously improve the corrosion resistance of the FHAP/MAO/Ti.

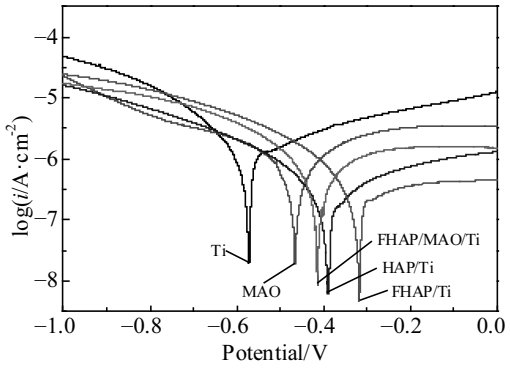

Fig.5 Potentiodynamic polarization (PDP) curves of CPTi, MAO/Ti, HAP/Ti, FHAP/Ti and FHAP/MAO/Ti

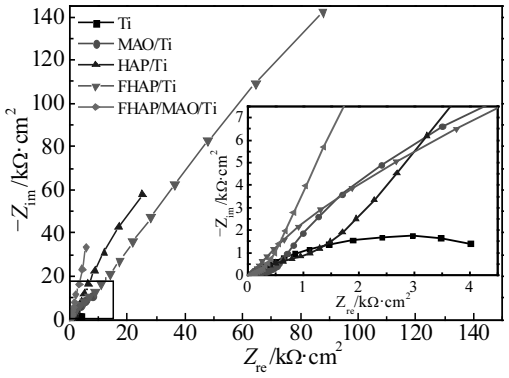

Fig.6 Nyquist plots of CPTi, MAO/Ti, HAP/Ti, FHAP/Ti and FHAP/MAO/Ti

Table 1 Electrochemical parameters of the samples obtained from the polarization curves

Sample	E_{corr}/mV	i_{corr}/μA·cm^{-2}
CPTi	–573	1.269
MAO/Ti	–967	2.822
HAP/Ti	–392	0.464
FHAP/Ti	–331	0.147
FHAP/MAO/Ti	–407	1.087

Furthermore, compared to that of the uncoated CPTi, the E_{corr} of HAP/Ti, FHAP/Ti increased from –573 mV (vs. SCE) to –392 mV (vs. SCE) and –331 mV (vs. SCE), respectively. The i_{corr} of HAP/Ti, FHAP/Ti decreased from 1.269 μA/cm^2 to 0.464 μA/cm^2 and 0.147 μA/cm^2, respectively. Thermodynamically, a higher corrosion potential indicates higher chemical inertness and better corrosion resistance[25]; thus, the anticorrosive properties of the specimens follow the order: FHAP/Ti> HAP/Ti>FHAP/MAO/Ti>MAO/Ti>CPTi. This results suggest that all the coatings provide a good protection and the FHAP/Ti shows better corrosion resistance.

2.5 Electrochemical impedance spectroscopy measurements

The Nyquist curves and Bode plots of uncoated CPTi, MAO/Ti, HAP/Ti, FHAP/Ti and FHAP/MAO/Ti of are shown in Fig.6 and Fig.7, respectively. As can be seen, the Nyquist curves (Fig.6) show a single semicircle for all the specimens. The real axis interception in the Nyquist curves can be ascribed to the solution resistance (R_s) and the charge transfer resistance (R_{ct}) due to the lower frequencies[26]. The impedance spectra of MAO/Ti, HAP/Ti, FHAP/Ti and FHAP/MAO/Ti are bigger than that of the uncoated CPTi, indicating an improved corrosion resistance of uncoated CPTi. The corrosion resistance of FHAP/MAO/Ti was significantly improved compared with that of the MAO/Ti, which shows that FHAP layer can significantly improve the corrosion resistance of MAO/Ti. This result is also consistent with the results of the polarization curve. Bode plot (log$f$ versus phase angle, Fig.7b for CPTi shows a fairly single peak, indicating only one

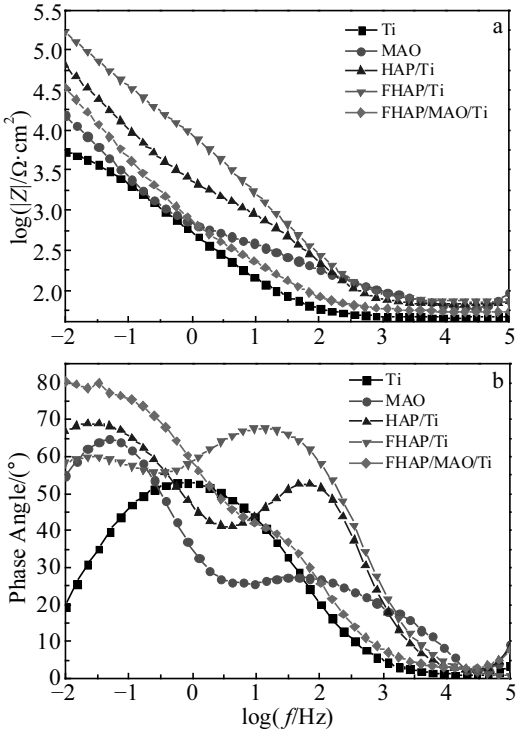

Fig.7 Bode plots of CPTi, MAO/Ti, HAP/Ti, FHAP/Ti and FHAP/MAO/Ti: log|Z| vs. log$f$ (a) and phase angle vs. log$f$ (b)

time constant existing at the interface between substrate and electrolyte (substrate/electrolyte). However, the curves of the MAO/Ti, HAP/Ti, FHAP/Ti and FHAP/MAO/Ti in Fig.7b show two peaks, which implies that there are two interfaces existing between substrate and electrolyte (coating/electrolyte and substrate/electrolyte) due to some micro-cracks and tiny pores on the surface of coatings. Moreover, the peaks at the low and high frequency regions correspond to equivalent capacitance of coatings (C_{coat}) and double layer capacitance (C_{dl}), respectively. Fig.7a shows that the log|Z| varies with the log frequency. The absolute impedance value increases in the

following order: FHAP/Ti>HAP/Ti>FHAP/MAO/Ti>MAO/Ti>CPTi, which implies that the FHAP/Ti exhibits higher corrosion resistance.

The equivalent electric circuit for uncoated CPTi and coated samples is shown in Fig.8. The equivalent electric circuit in Fig.8a was used to fit the impedance spectra of uncoated CPTi. It consists of a double layer capacitance (C_{dl}), a charge transfer resistance (R_{ct}), and a solution resistance (R_s). The rate of the electrochemical processes is controlled by the R_{ct} which is the key factor in determining the corrosion resistance[27,28]. The constant phase element (CPE) was introduced to replace C_{dl} in the proposed model. The admittance of CPE is defined as[29]:

$$Y_{CPE} = Y_0(j\omega)^n = Y_0\omega^n \cos\frac{n\pi}{2} + jY_0\omega^n \sin\frac{n\pi}{2} \quad (2)$$

where j is the imaginary unit ($j=\sqrt{-1}$), and ω is the angular frequency ($\omega=2\pi f$, f is the frequency). The coefficient Y_0 is an adjustable parameter used in the non-linear least squares fitting, and the coefficient n is between 0.5 and 1.

When the coated samples are soaked in the electrolyte, micro-cracks and tiny pores on the surface of coatings provide the direct diffusion path for the corrosive media. The galvanic-type corrosion cells are formed in this process, and the localized corrosion plays a dominant role in the corrosion process. In this situation, electrochemical interface can be divided into two sub-interfaces (electrolyte/coating and electrolyte/substrate). The impedance spectra was fitted using different equivalent electric circuits for such a system, as illustrated in Fig.8b, where R_{coat} is the coating resistance and C_{coat} is the equivalent capacitance of coating, R_s is the solution resistance, R_{ct} is the charge transfer resistance and the constant phase element (CPE) is also introduced to replace C_{coat}. Table 2 shows the values deduced using the equivalent circuit along with goodness of fit for both the CPTi and coated samples. The fitted results show that the sample prepared by MAO has low R_{coat} and R_{dl}. The value of R_{coat} decreases as the content of residual electrolyte inside the pores increases. After FHAP film was deposited on the MAO layer, the values of R_{coat} and R_{ct} increased from 454 Ω·cm^2 and 30.3 kΩ·cm^2 to 840 Ω·cm^2 and 223.3 kΩ·cm^2, respectively. This result indicates that the addition of FHAP decreases the porosity of MAO layer and improves the anticorrosion ability of CPTi. For FHAP/Ti and HAP/Ti, the value of R_{ct} is three orders of magnitude higher than that of the uncoated CPTi. This result indicates that the interface layer between the FHAP (HAP) layer and the substrate is primarily responsible for protecting the Ti substrate from electrical corrosion. In addition, the R_{ct} increases in the following order: HAP/Ti>FHAP/Ti>FHAP/MAO/Ti>MAO/Ti>CPTi, which also shows that the all the coatings provide effective protection for the Ti substrate.

2.6 SEM analysis after potentiodynamic polarization test

Fig.9 depicts the SEM micrographs of the surface of HAP/Ti (Fig.9a and 9b), FHAP/Ti (Fig.9c and 9d), and FHAP/MAO/Ti (Fig.9e and 9f) after PDP test in the simulated Hank's solution at 37 °C. From Fig.9a and 9b, breakages and micropores (marked by white circles) are clearly detected on the surface of HAP/Ti, which is because PDP test accelerates the release of hydrogen and formation of cracks. As shown in Fig.9c and 9d, the FHAP/Ti shows less corroded areas and cracks than the HAP/Ti, indicating that the presence of F improves the corrosion resistance of HAP. In addition, the FHAP/MAO/Ti retains the original surface morphology without corrosion pits after the PDP test (Fig.9e and 9f). Compared with HAP/Ti, it can be noticed that FHAP/Ti and FHAP/MAO/Ti show more intact surface than HAP/Ti, indicating that FHAP has better corrosion resistance than HAP, which is also in agreement with the PDP analysis.

Uncoated CPTi contacts the corrosive media directly, so it has a low corrosion resistance. MAO/Ti is soaked in the electrolyte, and corrosive media can permeate into substrate through outer loose layer. FHAP film was formed on MAO layer surface, then pores were filled and corrosion resistance was further improved. When FHAP or HAP film was deposited on CPTi surface, it can protect substrate from direct contact with electrolyte. Moreover, compared with HAP film, FHAP film can provide a lower dissolution rate and lower solubility in the body fluid[30], and FHAP layer can be more stable in electrolyte.

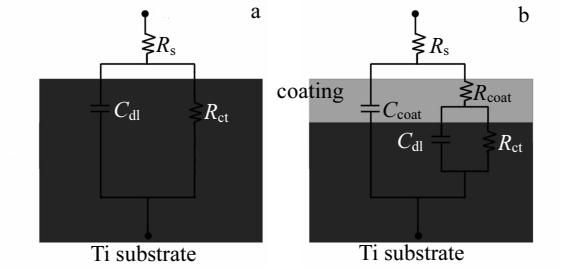

Fig.8 Equivalent circuit for uncoated CPTi (a) and coated samples (b)

Table 2 EIS data obtained by equivalent circuit simulation of uncoated and coated pure Ti samples

Sample	R_s/Ω·cm^2	CPE1		R_{coat}/kΩ·cm^2	CPE2		R_{ct}/kΩ·cm^2
		C_{coat}/×10^{-5} Ω^{-1}·cm^{-2}·s^{-n}	n_{coat}		C_{dl}/×10^{-5} Ω^{-1}·cm^{-2}·s^{-n}	n_{dl}	
Pure Ti	67.31	–	–	–	2.06	0.88	80.7
MAO/Ti	55.63	1.32	0.80	0.454	1.94	0.91	30.3
HAP/Ti	66.77	2.49	0.83	1.531	1.19	0.78	1056.1
FHAP/Ti	71.79	2.50	0.82	23.255	2.74	0.71	1237.1
FHAP/MAO/Ti	55.68	1.13	0.81	0.840	1.20	0.84	223.3

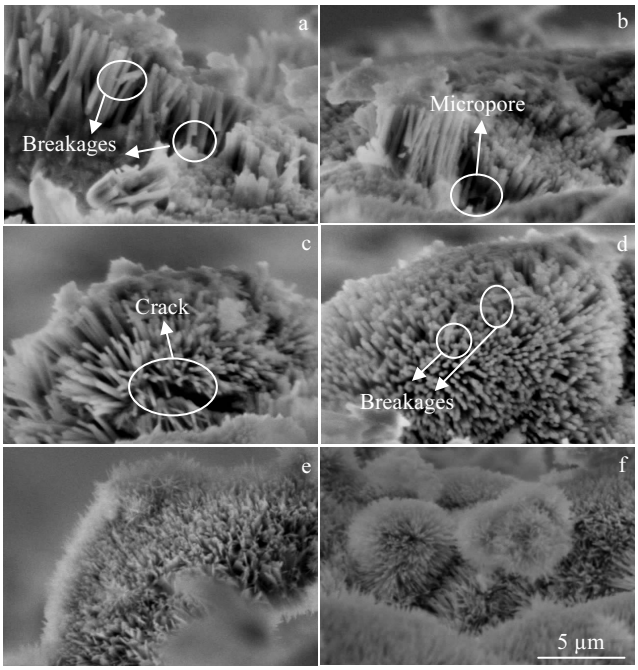

Fig.9 SEM images of HAP/Ti (a, b), FHAP/Ti (c, d) and FHAP/MAO/Ti (e, f) after potentiodynamic polarization in the simulated Hank's solution

2.7 Bonding strength, micro-hardness and modulus analysis

The bonding strength values between modified substrate and HAP coating of HAP/Ti, FHAP/Ti and FHAP/MAO/Ti coatings are reported in Fig.10a. The measured bonding strength of FHAP/MAO/Ti is about 18.1 MPa, which is higher than that of HAP/Ti (10.7 MPa) and FHAP/Ti (8.9 MPa). This result indicates that the bonding strength increases when a MAO layer is installed between the Ti substrate and FHAP layer because the pore configurations of MAO layer accelerate the migration and diffusion of ions, and the apatite nuclei will be formed when the ions are supersaturated on the three-dimensional porous structure surface[31]. Consequently, a great deal of apatite crystals are formed on the surface of porous MAO layer and the cohesive strength between MAO layer and HAP layer becomes higher. Fig.10b shows the elastic modulus and nanoindentation hardness of prepared uncoated CPTi and coated specimens. It is clearly observed that MAO/Ti has a higher nanoindentation hardness value (7.3 GPa) than other coated samples, while the hardness of coating obviously decreases with the addition of FHAP outer layer in the MAO coating. Furthermore, elastic moduli of the HAP/Ti (20.1 GPa), FHAP/Ti (25.7 GPa) and FHAP/MAO/Ti (17.7 GPa) coatings are similar, which are consistent with the reported elastic modulus of cancellous bone of 10~40 GPa[32]. The results suggest that the FHAP (HAP) deposited film on CPTi or single MAO layer surface can significantly improve biological integration and adjust the mechanical properties to comply with the natural bone system. In addition, analyses indicate that the FHAP/MAO/Ti has a better mechanical property than other samples.

2.8 Wettability test

The contact angles for HAP/Ti, FHAP/Ti, FHAP/MAO/Ti and uncoated CPTi are shown in Fig.11. Clearly, the coated specimens have smaller contact angles than CPTi (85.6°, Fig.11a). The value of contact angle decreases in the following order: CPTi>HAP/Ti>FHAP/Ti>FHAP/MAO/Ti, which indicates that FHAP/MAO/Ti has a lower contact angle. It also suggest that the hydrophobic surface of CPTi becomes hydrophilic after being coated with FHAP/MAO double layer, HAP coating (76.4°, Fig.11b) or FHAP coating (71.6°, Fig.11c). This result is attributed to the uneven FHAP/MAO interface and porous top surface of the FHAP with porous MAO as an interlayer (Fig.2d), which in turn can lead to an decrease in contact angle because of its increased roughness[33]. Kunzler et al[34] studied the cell response of osteoblasts to surface roughness by continuous variation in roughness values, and with the increase of surface roughness, osteoblasts showed a significant increase in proliferation rate. Bakhsheshi-Rad et al[35] showed that cell adhesion increases as the roughness of HAP coating increases. Similar report[36] shows that mammalian cells can be easily attached to the surface with small water contact angle (hydrophilic surfaces). Thus, the double-layer FHAP/MAO/Ti with higher hydrophilicity is more favorable for the cell attachment and proliferation.

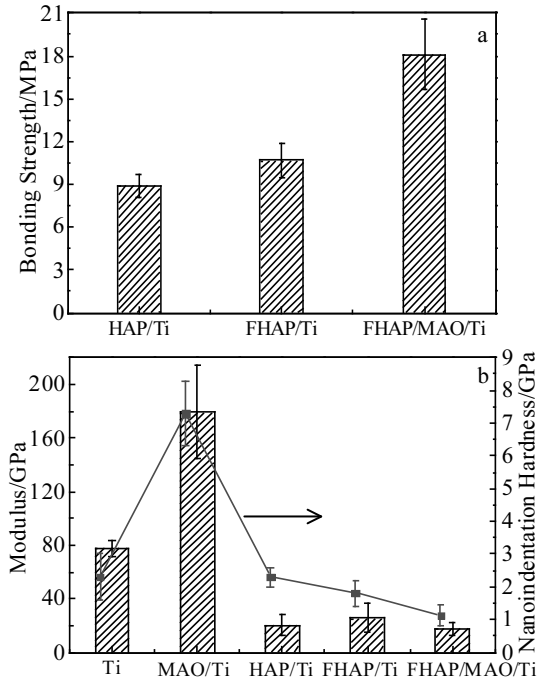

Fig.10 Bonding strength of the coatings estimated according to ASTM-C633 (a); elastic modulus and nanoindentation hardness of the uncoated CPTi substrate and coated specimens (b)

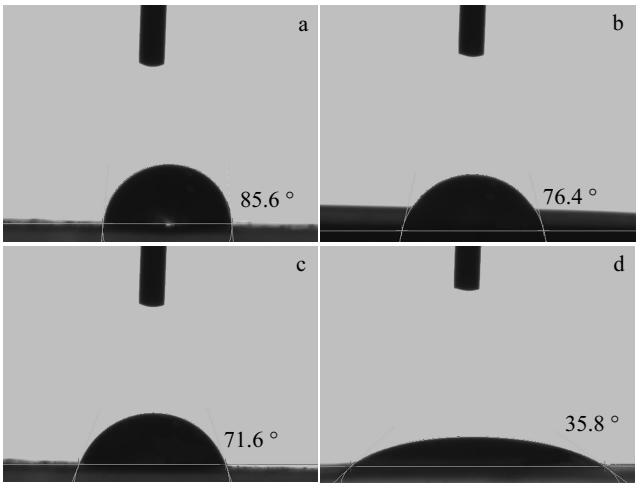

Fig.11 Contact angle of CPTi (a), HAP/Ti (b), FHAP/Ti (c), and FHAP/MAO/Ti (d)

3 Conclusions

1) The incorporation of F ion into the HAP structure induces an increase in the crystallinity of HAP and other phases. All the coating dramatically increases the corrosion resistance of CPTi, and FHAP/Ti has the best corrosion resistance of −331 mV (vs. SCE) in the Hank's solution.

2) The corrosion resistance of FHAP/Ti is also higher than that of other coated samples and CPTi, which indicates that the incorporation of the FHAP layer enhances the corrosion behavior of the MAO coating significantly. The bonding strength values between modified substrate and FHAP coating increase when a MAO layer is installed between the Ti substrate and FHAP layer.

3) FHAP/MAO/Ti exhibits better mechanical property than other samples. The elastic modulus of HAP/Ti (20.1 GPa), FHAP/Ti (25.7 GPa) and FHAP/MAO/Ti (17.7 GPa) are similar, which are also consistent with the reported elastic moduli of cancellous bone of 10~40 GPa. The contact angle of the FHAP/MAO/Ti is approximately 35.8°, which is more beneficial to promoting cell attachment and proliferation.

References

1 Bai Y, Park I S, Lee S J *et al. Applied Surface Science*[J], 2011, 257(15): 7010

2 Koch C F, Johnson S, Kumar D *et al. Materials Science & Engineering C*[J], 2007, 27(3): 484

3 Blind O, Klein L H, Dailey B *et al. Dental Materials*[J], 2005, 21(11): 1017

4 Xie J, Meng X, Zhou Z *et al. Materials Letters*[J], 2013, 110: 57

5 García F, Arias J L, Mayor B *et al. Journal of Biomedical Materials Research*[J], 1998, 43(1): 69

6 Tong W, Yang Z, Zhang X *et al. Journal of Biomedical Materials Research*[J], 1998, 40(3): 407

7 Song Y, Zhang S, Li J *et al. Acta Biomaterialia*[J], 2010, 6(5): 1736

8 Wang J, Chao Y, Wan Q *et al. Acta Biomaterialia*[J], 2009, 5(5): 1798

9 Heimann R B. *Surface & Coatings Technology*[J], 2006, 201(5): 2012

10 Uhlmann D R, Suratwala T, Davidson K *et al. Journal of Non-Crystalline Solids*[J], 1997, 218(97): 113

11 Alicja K, Małgorzata K, Grzegorz D *et al. Electrochimica Acta*[J], 2016, 204: 294

12 Bakhsheshi-Rad H R, Hamzah E, Daroonparvar M *et al. Vacuum*[J], 2014, 110: 127

13 Xu J L, Khor K A, Gu Y W *et al. Biomaterials*[J], 2005, 26(15): 2197

14 Frayssinet P, Hardy D, Rouquet N *et al. Biomaterials*[J], 1992, 13(10): 668

15 Mohan L, Durgalakshmi D, Geetha M *et al. Ceramics International*[J], 2012, 38(4): 3435

16 Fazel M, Salimijazi H R, Golozar M A *et al. Applied Surface Science*[J], 2015, 324: 751

17 Bakhsheshi-Rad H R, Hamzah E, Ebrahimi-Kahrizsangi R *et al. Vacuum*[J], 2016, 125: 185

18 Gnedenkov S V, Sinebryukhov S L, Mashtalyar D V *et al. Vacuum*[J], 2015, 120: 107

19 Rokosz K, Hryniewicz T, Raaen S. *International Journal of Advanced Manufacturing Technology*[J], 2015, 85(9): 2425

20 ASTM international. *Standard Test Method for Adhesion or Cohesion Strength of Thermal Spray Coatings*, ASTM C663-01 [S]. Philadelphia: West Conshohocken, 2001

21 He Daihua, Liu P, Liu X *et al. Journal of Wuhan University of Technology-Mater Sci Ed*[J], 2014, 29(2): 398

22 Sternitzke V, Kaegi R, Audinot J N *et al. Environmental Science & Technology*[J], 2012, 46(2): 802

23 Montazeri M, Dehghanian C, Shokouhfar M *et al. Applied Surface Science*[J], 2011, 257(16): 7268

24 Gu Y, Chen L, Yue W *et al. Journal of Alloys & Compounds*[J], 2016, 664: 770

25 Zhao Y, Wei L, Yi P *et al. International Journal of Hydrogen Energy*[J], 2016, 41(2): 1142

26 Zomorodian A, Garcia M P, Moura S T *et al. Acta Biomaterialia* [J], 2013, 9(10): 8660

27 Grips V K W, Selvi V E, Barshilia H C *et al. Electrochimica Acta*[J], 2006, 51(17): 3461

28 Bakhsheshi-Rad H R, Hamzah E, Ismail A F *et al. Journal of Alloys & Compounds*[J], 2015, 648: 1067

29 Zoltowski P. *Journal of Electroanalytical Chemistry*[J], 1998, 443(1): 149

30 Bakhsheshi-Rad H R, Hamzah E, Daroonparvar M *et al. Transactions of Nonferrous Metals Society of China*[J], 2014, 24(8): 2516

31 He D H, Wang P, Liu P *et al. Surface & Coatings Technology*[J], 2015, 277: 203

32 Gibson L, Ashby M. *Cellular Solids Structure and Properties*[M].

Sydney: Pergamon Press, 1988
33 Lee H U, Jeong Y S, Park S Y *et al. Current Applied Physics*[J], 2009, 9(2): 528
34 Kunzler T P, Drobek T, Schuler M *et al*. *Biomaterials*[J], 2007, 28(13): 2175
35 Bakhsheshi-Rad H R, Hamzah E, Ismail A F *et al. Ceramics International*[J], 2016, 42(10): 11 941
36 Gopi D, Karthika A, Rajeswari D *et al. Rsc Advances*[J], 2014, 66: 34 751

基于微弧氧化和电化学沉积在纯 Ti 基体表面制备 FHAP/MAO 复合涂层的腐蚀行为和力学性能

金　杰，周树伟，郑大才
(浙江工业大学，浙江 杭州 310014)

摘　要：采用微弧氧化和电化学沉积（ED）技术在工业纯钛（CPTi）表面沉积氟掺杂羟基磷灰石 (FHAP)/微弧氧化（MAO）复合涂层。并在 Hsnk's 溶液中对未涂覆的 CPTi 基材和涂覆的样品进行电化学耐腐蚀性测试。研究了 MAO 界面层对涂层微观结构，力学性能和电化学性能的影响。结果表明，HAP/Ti，FHAP/Ti 和 FHAP/MAO/Ti 复合涂层样品在模拟 Hank's 溶液中提高了 CPTi 基体的耐腐蚀性能。然而，力学性能测试表明，与具有 MAO 界面层的 FHAP/Ti 涂层的结合强度（18.1 MPa）相比，FHAP/Ti 涂层的结合强度较差（10.7 MPa）。此外，FHAP/MAO/Ti 涂层的接触角约为 35.8°，这更有利于促进细胞附着和增殖。

关键词：羟基磷灰石；微弧氧化；耐腐蚀性；电化学测试；接触角

作者简介：金　杰，男，1960 年生，博士，教授，浙江工业大学材料科学与工程学院，浙江 杭州 310014，E-mail: jiejinzjut@sina.com